Energy 198 (2020) 117379

Contents lists available at ScienceDirect

Energy

journal homepage: www.elsevier.com/locate/energy

Proposal and analysis of an integrated solar combined cycle with partial recuperation

Antonio Rovira [a, *], Rubén Abbas [b], Consuelo Sánchez [a], Marta Muñoz [a]

[a] Universidad Nacional de Educación a Distancia, UNED, Spain
[b] GIT-ETSII – Universidad Politécnica de Madrid, UPM, Spain

ARTICLE INFO

Article history:
Received 6 December 2019
Received in revised form
6 February 2020
Accepted 12 March 2020
Available online 18 March 2020

Keywords:
ISCC
Hybridization
Combined cycle
CSP
Partial recuperation

ABSTRACT

The paper analyses an integrated solar combined cycle that, as a novelty, includes a gas turbine with partial recuperation. A conventional solar arrangement including parabolic troughs with a thermal oil is assumed. This field feeds a solar steam generator working in parallel with the high-pressure evaporator of the heat recovery steam generator. The plant is designed to balance out the solar supply to the steam cycle with the thermal power transferred to the air in the recuperator before it is introduced in the combustion chamber. Thus, only a fraction of the turbine exhaust gas flows through the recuperator. The additional steam production due to the solar contribution is mitigated by lower power available at the evaporator of the heat recovery steam generator, making possible to achieve constant steam turbine operation regardless the solar contribution. Results show that the proposal reaches better performance and lower generating cost than conventional integrated solar combined cycles. Besides, a new proposal to evaluate plant performances and economical assessments is introduced, which has been shown useful to understand correctly the results obtained.

1. Introduction

Conventional thermal power plants will still have an important share in the grid mix in the medium term. When both conventional thermal plants and concentrating solar power (CSP) plants are present in the electricity mix, hybridization of both sources is more convenient in terms of an efficient use of fossil fuels. In addition, hybridization leads to advancing on the CSP learning curve while minimizing investment risks thanks to the fossil fuel supply. This might be done by means of integrated solar combined cycles (ISCC).

This technology has been studied since the late 90s. Designs of the early studies were based on the parabolic trough technology (PTC) developed for the SEGS plants [1]. At the beginning of this century, interest in ISCC increased because of the construction of some plants granted by the Global Environment Facility agency to developing countries like Egypt, Morocco, India and Mexico [2].

Up to date, a small number of ISCC have been put into operation worldwide, like Aïn Beni Mathar (Morocco), Hassi R'mel (Algeria), Kuraymat (Egypt), Martin Next Generation Solar Energy Center (USA), Agua Prieta II (Mexico), Archimede (Italy) and Yazd (Iran). There are others planned or in construction, like Ningxia (China), Palmdale Hybrid Power Plant and Victorville 2 Hybrid Power Plant (USA), Abdaliya (Kuwait) or Duba 1 ISCC (Saudi Arabia) [3,4].

Studies like Dersch's et al. [5] show the domain of PTC technology within ISCC. In most cases, the solar heat is transferred to the water/steam of the bottoming cycle using a solar steam generator (SSG) that is fed by the heat transfer fluid (HTF). This HTF is usually a thermal oil [3], although other choices like the use of molten salts [6] has been used. Direct steam generation (DSG) has been also proposed [7,8], leading to higher efficiency but lower reliability. Furthermore, some authors have proposed the use of CO_2 as HTF [9], although the results were not successful in the economic framework established.

In the state-of-the-art configurations, the solar thermal input is transferred to the steam cycle for high-pressure evaporation [3,10] and, in some cases, a slight degree of superheating [11,12], pre-heating [13] or both superheating and pre-heating [6]. There are also studies that propose the solar integration at the low or intermediate pressure level of the Heat Recovery Steam Generator (HRSG). For example, Calise et al. [14] suggest the use of PTC using thermal oil to increase the steam production of the low-pressure level. The reasons that support the integration at this level are a

* Corresponding author.
E-mail addresses: rovira@ind.uned.es (A. Rovira), ruben.abbas@upm.es (R. Abbas), csanchez@ind.uned.es (C. Sánchez), mmunoz@ind.uned.es (M. Muñoz).

https://doi.org/10.1016/j.energy.2020.117379

Nomenclature

Acronyms

CCGT	Combined cycle gas turbine
CSP	Concentrating solar power
CTR	Central tower receiver
DSG	Direct steam generation
HP	High pressure
HTF	Heat transfer fluid
HRSG	Heat recovery steam generator
ISCC	Integrated solar combined cycle
ISCC-PR	Integrated solar combined cycle with partial recuperation
LP	Lower pressure
O&M	Operation and maintenance
PR	Partial recuperation
PTC	Parabolic trough collector
SSG	Solar steam generator
TMY	Typical meteorological year

Symbols

A	Area (m^2)
C	Cost of energy ($€\cdot J^{-1}$)
c_p	Specific heat at constant pressure ($J\cdot kg^{-1}\cdot K^{-1}$)
DNI	Direct normal irradiation ($W\cdot m^{-2}$)
IAM	Incidence angle modifier (−)
e	Specific exergy ($J\cdot kg^{-1}$)
E	Energy (J)
$\dot{E}$	Exergy flow (W)
h	Specific enthalpy ($J\cdot kg^{-1}$), hour
H_c	Heating value ($J\cdot kg^{-1}$)
HR	Heat rate (−)
Inv	Investment (€)
K	Steam turbine mass flow parameter ($\dot{m}_{st}\cdot\sqrt{T_i/(p_i^2-p_o^2)}$) ($m\cdot K^{0.5}$ s)
L	Length (m)
LC	Levelized cost (€)
$LCOE$	Levelized cost of electricity ($€\cdot J^{-1}$)
$\dot{m}$	Mass flow ($kg\cdot s^{-1}$)
n	Yearly frequency of a determined operating condition (−)
p	Pressure (Pa)
P	Power (W)
$\dot{Q}$	Thermal power (W)
t	Time interval (1 h)
T	Temperature (K)
U	Overall heat transfer coefficient ($W\ K^{-1}\ m^{-2}$)
W	Width (m)
x	Mass flow ratio (−)

Greek letters

Δ	Increment
ε	Recuperator effectiveness (−)
ξ	Pressure drop (−)
η	Efficiency (−)

Subscripts

a	Air
col	Collector
des	Design
ec	Economizer
ev	Evaporator
f	Fuel
gt	Gas turbine
g	Gas
i	Inlet
inc	Incremental
ise	Internal solar-to-electricity
l	Local coordinate of the PTC
max	Maximum
net	Net
o	Outlet
R	Recuperator
sh	Superheater
sol	Solar
$sol\text{-}elec$	Solar-to-electricity
st	Steam turbine

better sizing of the heat exchangers and a better integration in the steam turbine. Brodrick et al. [15] study the behaviour of an ISCC in which the solar thermal power is integrated at the intermediate-pressure level of the HRSG, and the control of the HTF temperature, concluding that, in the case of ISCC, a strategy varying this temperature can be interesting. Li and Yang [8] propose, in a first work, the introduction of the solar heat in two stages: one at the high-pressure level and the other at the low-pressure one, working in both cases with DSG. In a second work [16], they propose the change of the PTC dedicated to the low-pressure level steam generator by evacuated flat collectors. Finally, Bonforte et al. [17] study the solar heat introduction in all pressure levels (70 MW for the high-pressure level, 20 MW for the intermediate-pressure one and 40 MW for the low-pressure one).

Regarding the integration point within the combined cycle, as commented, the most common choice is to introduce the solar heat to the steam cycle, although other options have been also studied. The use of PTC to preheat the air of the gas turbine before it is introduced in the combustion chamber is put forward in Refs. [18], where authors proposed air preheating up to 580 °C to achieve a yearly fuel saving of 15.5%. In Ref. [19], the same integration point is proposed but using a central tower receiver (CTR) system to preheat the air. The use of a CTR is also suggested in Refs. [20], in this case to add a stream of hot air to the exhaust gas coming from the gas turbine outlet.

Duan et al. [21] also propose the solar integration for air preheating at the exit of the compressor. Unlike in Refs. [18,19], in this case the air is preheated after it preheats, in turn, the water of the steam cycle. Thus, the temperature of the air within the receiver is lower. The air is heated up again to a temperature higher than the compressor outlet one, so the configuration can benefit from higher production and lower fuel consumption simultaneously.

Rovira et al. [22,23] compare the yearly behaviour of different ISCC and hybrid systems working with different solar concentrating technologies: PTC, linear Fresnel collectors and CTR integrating solar energy either to the bottoming cycle or to the air of the gas turbine. These works show that configurations with solar integration at the bottoming cycle (i.e. conventional ISCCs) lead to higher yearly production and use more conventional and reliable solar concentrating technologies (for example, PTC). However, configurations with solar integration at the gas turbine lead to significantly higher solar-to-electricity efficiencies (even higher than 50%), but

with less reliable solar concentrating technologies.

Regarding the high solar-to-electricity efficiency, Rovira et al. [24] present a layout for the ISCC based on the concept of partial recuperation (PR) for the gas turbine, previously analysed in Refs. [25] for combined cycle gas turbines (CCGT) without solar integration. Partial recuperation can lead to reduce the fuel consumption without varying the gas turbine operating conditions and, thus, without reducing its efficiency. The introduction of partial recuperation into ISCC allows the use of conventional solar concentrating technologies (PTC with HTF), where solar input is introduced at the bottoming cycle (as in conventional ISCC) and, at the same time, a fuel saving equivalent to non-conventional technologies with solar integration into the gas turbine. Therefore, this configuration can operate with reliable technology and, simultaneously, lead to solar-to-electricity efficiencies higher than 50% (in net terms). Although this configuration was presented in previous works [24] and a similar concept has been studied without solar integration [25], a complete analysis of its annual performance and cost has never been carried out. This study would allow to rate the proposed configuration with state-of-the-art CCGT and ISCC.

The main objective of the present work is to study in detail and for the first time the original ISCC proposal that follows the layout presented in Ref. [24]. The goal is to enlarge synergies between combined cycle and solar technologies, increasing the performance over conventional ISCCs in terms of efficiency and costs. The configuration is based on a CCGT with HRSG of two pressure levels, and solar heat integration within the steam cycle in parallel to the evaporator of the high-pressure level. The solar concentrating technology is PTC using a thermal oil as HTF. The study includes the analysis of the yearly performance and the economical assessment.

As a secondary objective, a discussion about the different figures of merit to assess the ISCC technology is carried out. At this regard, the conventional incremental solar-to-electricity efficiency will be used, together with a modified one defined in Ref. [8,24] and a new proposal developed for this work.

In Section 2 the reference configurations are presented. The proposed configuration is described in Section 3. Section 4 shows the methodology used in the analysis and the figures of merit. The results, including the preliminary sizing of the most relevant equipment, daily and yearly operation analysis are presented in Section 5. Finally, Section 6 shows the conclusions.

2. Reference configurations

2.1. Reference combined cycle gas turbine

In order to make comparisons, a conventional CCGT without solar integration is defined as a reference power plant. In this configuration, the exhaust gas of the gas turbine is directed to a double pressure-level HRSG that feeds the steam turbine of the Rankine cycle. Fig. 1 shows the scheme of the layout, while Table 1 presents the main design parameters of the configuration.

2.2. Reference integrated solar combined cycle

In order to compare the proposed configuration with a conventional ISCC, a reference ISCC is also established. The layout of the configuration is presented in Fig. 2. As it can be observed, the reference ISCC is based on the reference CCGT, where a solar field with PTC is included. PTC heats up a thermal oil, in this case Therminol VP1, which is used to feed the SSG. The SSG works in parallel to the evaporator of the high-pressure level of the HRSG, increasing the high-pressure steam production when the solar field is operating.

Table 1 also presents the main design parameters of the reference ISCC, and Table 2 shows the main features of the PTC solar field. Solar thermal power is set to 16 MW_{th} at nominal conditions (net term).

3. Integrated solar combined cycle with partial recuperation

The objective of the integrated solar combined cycle with partial recuperation, namely ISCC-PR, is to allow fuel savings equivalent to the introduced solar heat by means of a recuperative heat exchanger in the gas turbine and, at the same time, to maintain the steam production constant. Fig. 3 depicts the layout of the configuration. The gas turbine exhaust is divided into two main streams: one stream is directed to the high-pressure part of the HRSG, whereas the other is directed to the recuperator and, then, to the high-pressure evaporator inlet, where both streams are mixed.

As in the case of the reference ISCC, the solar field consists on a set of PTC working with a thermal oil (Therminol VP1) that is used to evaporate water of the high-pressure level, in parallel to the corresponding evaporator of the HRSG.

The fraction of gas turbine exhaust flow that is directed to the recuperator is selected to make equal the thermal power exchanged in the heat exchanger and the thermal power supplied by the solar field to the high-pressure evaporator at the design point. Besides, as the temperature of gas coming from the gas turbine at the superheater inlet is the same as in CCGT and ISCC cases, the high pressure steam temperature can be the same as in these reference configurations.

One may observe in Fig. 3 that there are two bypasses at the recuperator: one at the exhaust gas side and the other at the air side. As mentioned, the thermal power exchanged in the recuperator can modulated by varying the gas fraction that goes through the recuperator. With the goal of maintaining constant the gas mass fraction that goes to the superheater regardless the gas mass fraction directed to the recuperator and the solar contribution, a bypass at the gas side (dotted line in Fig. 3) is introduced. Thus, once a gas mass fraction is sent to the recuperator, the bypass deviates another fraction before entering the superheater, in such a way that the sum of both mass flow rates (through the recuperator and through the bypass) is constant and, consequently, gas mass flow directed to the superheater is also constant. Besides, the bypass at the air side allows an air flow modulation to achieve constant temperature difference at the two ends of the recuperator.

Moreover, the fact that the thermal power transferred in the recuperator and the solar thermal power are equal also allows constant steam production at the HRSG, because each thermal unit added by the solar field to the water/steam is removed from the gas contribution in the evaporator.

The design parameters of the different equipment are shown in Table 1 and Table 2. The solar thermal power is set to 16 MW_{th} and the effectiveness of the recuperator (ε) is 80%.

4. Methodology

Simulation of systems at nominal conditions is based on the mass and heat balances of each equipment at steady conditions. Therefore, some design and technological parameters are required in order to complete the information of the system. The following sub-sections describe the specific models used for the different equipment. The code of simulation models was implemented in Visual Basic. Refprop software is used for obtaining the thermophysical properties of involved fluids.

A dataset containing all the results of the work has been included as complementary material [26].

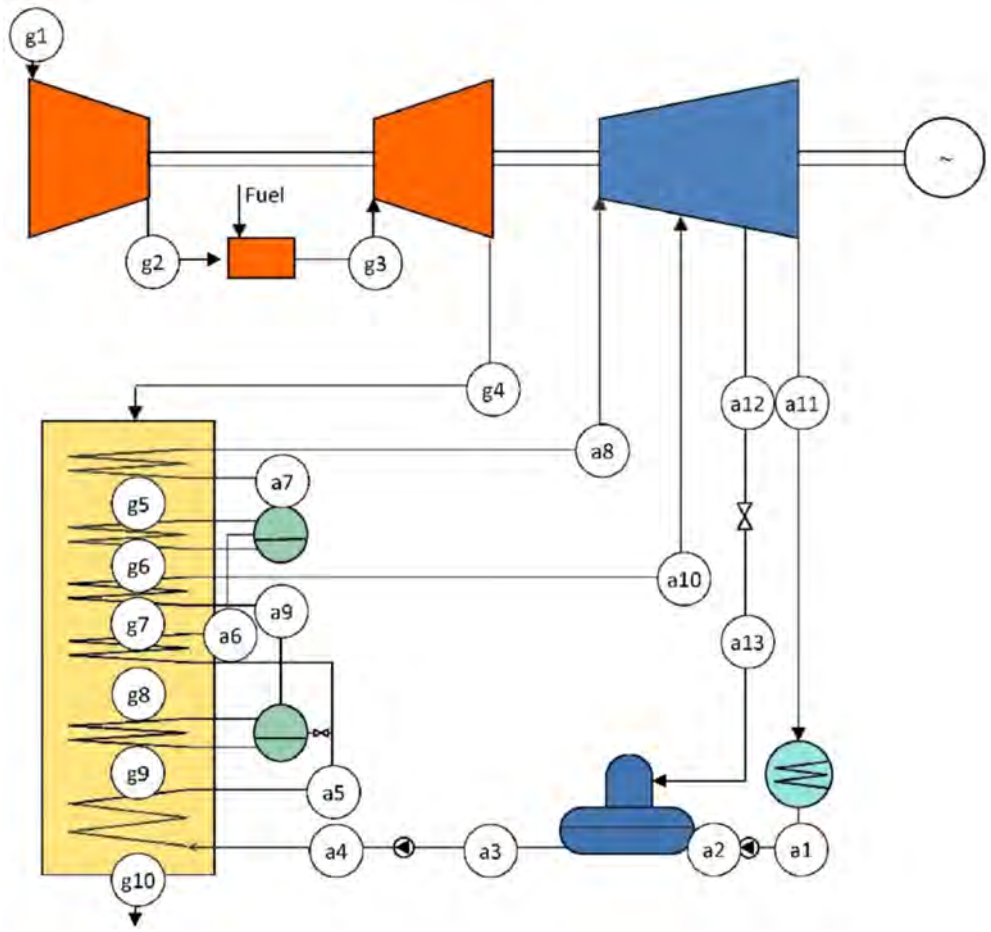

Fig. 1. Layout of the reference CCGT.

Table 1
Design parameters and nominal performance of the configurations.

Reference CCGT and ISCC configurations			
Ambient T and p	288 K, 1 bar	HP live steam T	818 K
Compressor pressure ratio	16:1	HP pressure level	90 bar
Compressor air mass flow	210 kg/s	HP pinch point	10 K
Gas turbine inlet temperature	1500 K	LP live steam T	566 K
Compressor polytropic efficiency	90%	LP pressure level	5 bar
Turbine polytropic efficiency	90%	LP pinch point	10 K
Steam turbine isentropic efficiency	85%	Combustion chamber efficiency	95%
Pumps isentropic efficiency	75%	Mechanical efficiency	98%

4.1. Simulation models for the gas turbine

In the case of the gas turbine, the compressor takes air from the environment and compresses it before it flows through the combustion chamber (reference CCGT and ISCC configurations) or through the recuperative heat exchanger (ISCC-PR configuration). The air outlet pressure is defined by the compressor pressure ratio (r_{gt}) and the pressure drop at the compressor inlet, which is set to 20 mbar.

Compression is simulated as an adiabatic and non-reversible process. Thus, a polytropic efficiency is considered (Table 1). The compressed air enters the combustion chamber together with the fuel (natural gas) assuming a pressure drop of 5%. Finally, the gases exiting the combustion chamber are directed to the turbine, where they expand in an adiabatic and non-reversible process. The pressure at the turbine outlet is known, since it is the ambient one plus a slight pressure drop at the HRSG. The considered pressure drop is 40 mbar. In order to consider the irreversibility, a polytropic efficiency is considered (Table 1).

In the case of the ISCC-PR configuration, the recuperator is also simulated. The corresponding heat balance is as follows:

$$x_a \cdot \dot{m}_a \cdot (h_{g2R} - h_{g2}) = x_g \cdot \dot{m}_g \cdot (h_{g4} - h_{g4R}) \quad (1)$$

In Equation (1), x_a is the ratio of air mass flow rate that is directed to the cold side of the recuperator to the total air mass flow rate (see Fig. 3), and x_g is the ratio of gas turbine exhaust gas that is directed to the hot side of the recuperator to the total exhaust gas mass flow rate.

Additionally, the effectiveness (ε) of the recuperator is required, that is defined as below:

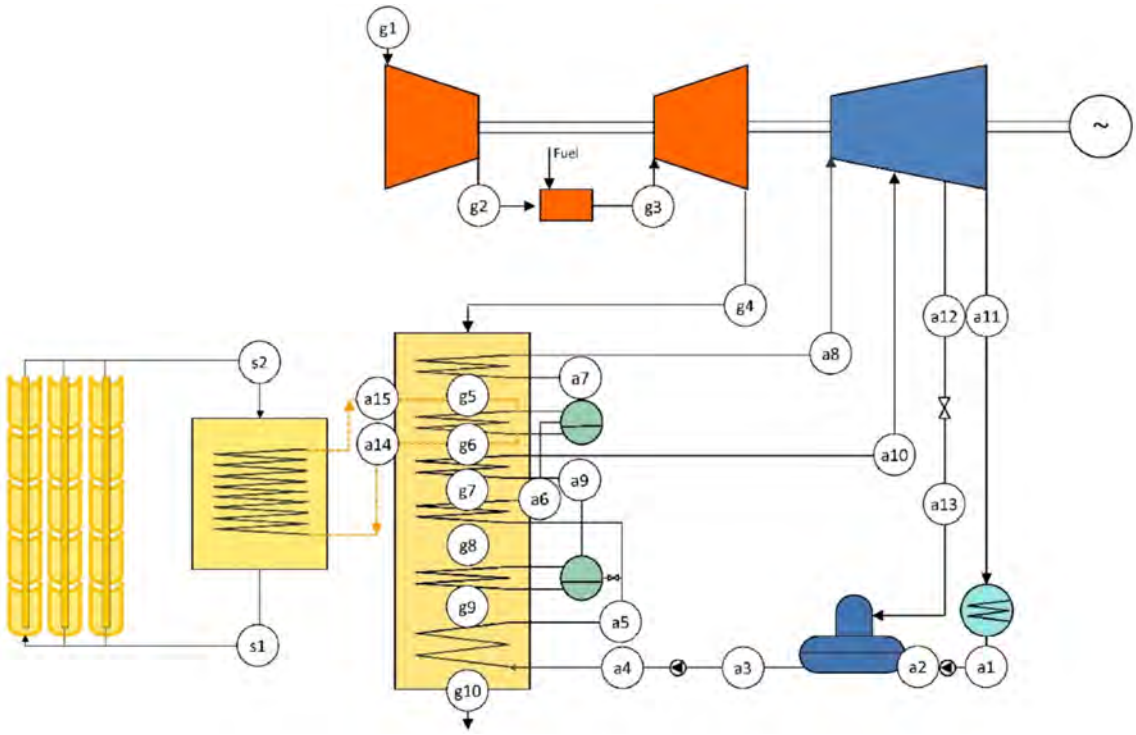

Fig. 2. Layout of the reference ISCC.

Table 2
Features of the solar field (PTC) at the design point.

Absorber tube outer diameter	0.07 m	Mirror reflectivity	92%
Absorber tube inner diameter	0.065 m	Glass transmisivity	94.5%
Glass envelope outer diameter	0.115 m	Solar absorptivity	94%
Glass envelope inner diameter	0.109 m	Peak optical efficiency	75%
Module length	12.27 m	Thermal emissivity	0.04795 + 0.0002331 T (°C)
Mirror length	11.9 m	Máximum $\dot{m}_{HTF}$ per loop	7.725 kg/s
Intercept factor	92%		

$$\varepsilon = \frac{T_{g2R} - T_{g2}}{T_{g4} - T_{g2}} \tag{2}$$

In Equation (2), the numerator represents the temperature variation of the stream with lowest heat capacity ($\dot{m} \cdot c_p$) in the recuperator. In this case it corresponds to the air. The denominator represents the maximum temperature variation.

The recuperator introduces an additional pressure drop at the air side. It is calculated with the following equation (obtained from Ref. [27]):

$$\xi = (\varepsilon - 0.48) / 30 \tag{3}$$

The additional pressure drop at the gas side is mitigated by a lower pressure drop in the HRSG, since the HRSG should exchange lower thermal power as the exhaust gas has exchanged part of its heat in the recuperator.

Thermo-physical properties of the air and the gas are calculated from Ref. [28].

For the off-design simulation of the gas turbine, specific simulation models should be used. Such operation takes place when ambient conditions are different from the nominal ones or in a scenario of part-load operation. In this work, the strategy is to maintain the gas turbine working at full load, so off-design operation is due to the variation of ambient conditions.

The off-design behaviour of the compressor is usually defined by its characteristic curves. These curves are based on Ref. [29]. Regarding the combustion chamber, as the gas turbine is maintained at the maximum possible load, the turbine inlet temperature is kept at its nominal value. As in the case of the compressor, the turbine behaviour is described by its characteristic curves [30].

Finally, in the case of the ISCC-PR configuration, the off-design behaviour of the recuperator can be characterised by means of the heat balance and its thermal conductance (UA) considering a counter-flow heat exchanger:

$$\dot{Q}_{R,gt} = UA \cdot \frac{(T_{g4} - T_{g2R}) - (T_{g4R} - T_{g2})}{ln((T_{g4} - T_{g2R})/(T_{g4R} - T_{g2}))} \tag{4}$$

The thermal conductance can be calculated at nominal conditions, and it varies at off-design operation. The variation can be assessed with the equation below [31]:

$$U \Big/ U_{des} = \left(\frac{x_a \cdot \dot{m}_a}{x_{a,des} \cdot \dot{m}_{a,des}} \right)^q \tag{5}$$

In flows with Prandtl numbers of roughly 0.7 the exponent q takes the value of 0.625.

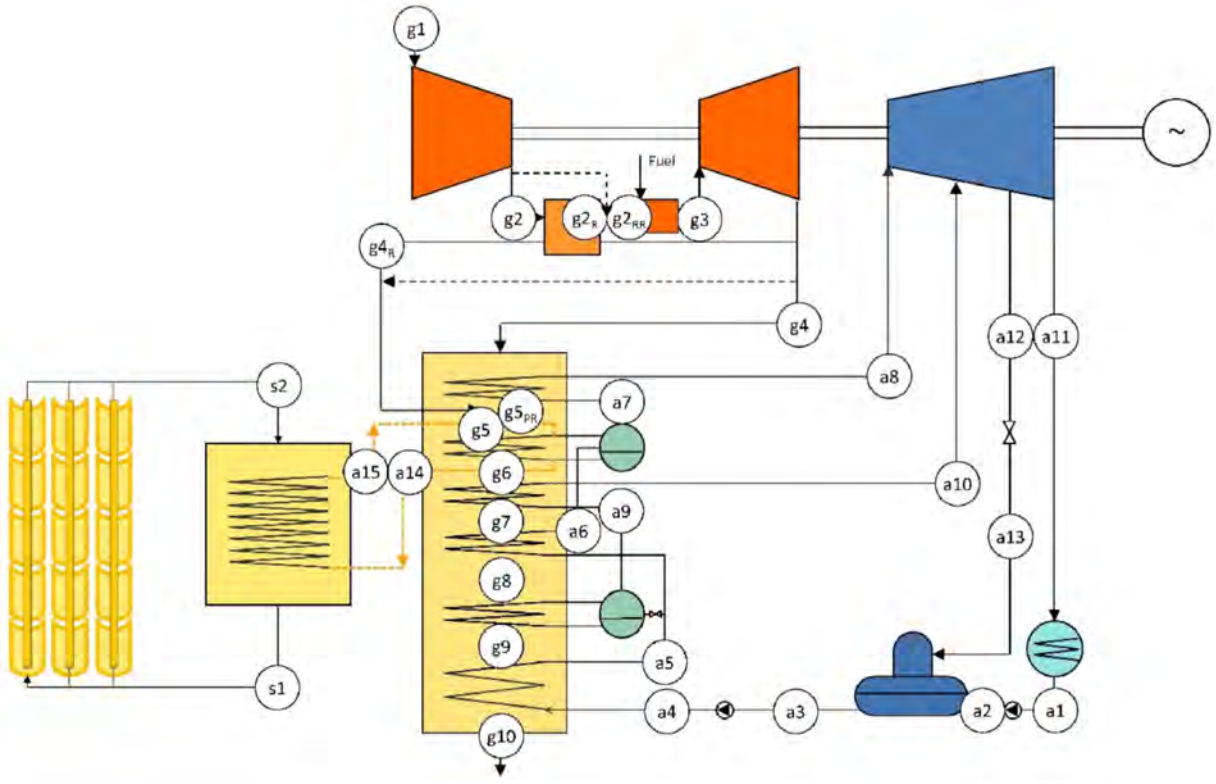

Fig. 3. Layout of the ISCC-PR.

4.2. Simulation models for the HRSG and steam turbine

Simulation models for the economisers, evaporators and superheaters of the HRSG are based on the energy balances. For the simulation at nominal conditions, some design parameters are also required (see Table 1). These are the steam temperature at the outlet of the superheaters, the pinch points for each pressure level, the approach points (fixed at 25 K), the working pressure at both pressure-levels and the temperature of the feedwater from the deaerator, which is established in 60 °C (corresponding to a saturation pressure of 0.2 bar).

In the ISCC-PR configuration, only a fraction of the exhaust gas from the gas turbine flows through the superheater. Assuming that the heat exchanger is balanced, the temperature difference at the cold- and hot-ends is the same, and the following heat balance can be established (numbering of Fig. 3):

$$x_{sh} \cdot \dot{m}_g \cdot (h_{g4} - h_{g5PR}) = \dot{m}_{HP} \cdot (h_{a8} - h_{a7}) \quad (6)$$

The gas mass flow rate that exits the superheater is mixed with the other fractions coming from the recuperator and the by-pass, resulting:

$$x_{sh} \cdot h_{g5PR} + x_g \cdot h_{g4R} + (1 - x_{sh} - x_g) \cdot h_{g4} = h_{g5} \quad (7)$$

On the other side, the steam leaving the high pressure superheater is expanded in the high pressure cylinder of the steam turbine. As the process is adiabatic and non-reversible, an isentropic efficiency of 85% is considered.

The steam at the exit of the high pressure cylinder of the steam turbine is mixed to that from the low-pressure superheater, and this total steam is directed to the low-pressure cylinder of the steam turbine. In this cylinder there is a steam extraction line at 1.2 bar that feeds the deaerator. The isentropic efficiency for this cylinder is also 85%.

The condensation pressure is fixed at 56 mbar, which corresponds to a saturation temperature of 35 °C, above the ambient temperature (20 °C). The condensate is pumped up to the deaerator pressure (0.2 bar), considering an isentropic efficiency for the pump of 75%.

Finally, the saturated water from the deaerator is pumped up to the high-pressure level plus an additional pressure drop of 5%.

For the off-design calculation of the HRSG, the thermal conductance of each heat exchanger is required together with the energy balances. The heat exchange equation is similar to Equation (4). In economisers and evaporators, the highest resistance to the heat exchange is found at the gas side flow. Thus, the variation of the overall convective heat exchange coefficient follows also Equation (5), but replacing $x \cdot \dot{m}_a$ by $\dot{m}_g$. In the case of superheaters, the convective heat exchange coefficients at the gas side and the steam sides are similar. In order to simplify the calculations, the variation expressed in Equation (5) is also used, which is commonly employed to avoid a complete design of the exchanger.

For the ISCC-PR configuration, the calculation of the gas mass flow rate that is directed to the superheater at each operating condition is required. The mass fraction that goes to the recuperator (x_g at g_{4R} conditions in Fig. 3) is selected to achieve a heat exchange equal to the thermal power introduced by the solar field. The fraction that goes to the superheater (x_{sh} at g_4 conditions in Fig. 3) is selected to generate the same steam mass flow as the CCGT at the same operating conditions. Finally, the remaining gas mass flow rate goes through the bypass and is mixed with the gas exiting the recuperator.

In order to assess the behaviour of the steam turbine at off-design operation, the Stodola-Frügel Law is used:

$$\dot{m}_{st} \cdot \sqrt{\frac{T_i}{p_i^2 - p_o^2}} = K \tag{8}$$

This law can be applied in each section or cylinder of the steam turbine in which the steam mass flow rate keeps constant. In the present study the sections are the high-pressure cylinder, the section from the inlet to the low-pressure cylinder to the extraction line, and the section from the latter to the outlet of the low-pressure cylinder.

Regarding the variation of the isentropic efficiency, in the technical literature there are different methodologies to assess it. In the present paper, the correlation used in Ref. [32] is implemented, which leads to a decrease of 10% points in the isentropic efficiency when the relative turbine capacity $((\dot{m} \cdot \sqrt{T_i}\ /p_i)/(\dot{m}_{des} \cdot \sqrt{T_{i,des}}\ /p_{i,des}))$ varies from 100% to 70%.

Finally, the condensation temperature follows the evolution of the ambient temperature. Specifically, for each unit in the ambient temperature variation the condensation one varies a half. This lower amplitude in the variation lies on the fact of condensers in CCGT and ISCC are usually cooled by water, with a temperature variation lower than the ambient one.

4.3. Simulation models for the PTC and the SSG

The solar field considered consists of several loops of Eurotrough 150 PTCs (ET-150). Main parameters were shown in Table 2 [33]. Models for the simulation of PTC are also based in the heat balances [33], which accounts for the energy gains from the solar energy, the heat transferred to the HTF and the losses: different optical errors and thermal losses to the environment (convection, conduction and radiation). Petukov's correlation is used to guess the convection losses and a thermal emissivity of 94% is considered for the radiation ones. Pressure drop is calculated with the Colebrook's equation.

Direct normal irradiation (DNI) at nominal conditions is set to 850 W/m^2. In the case of PTC cooled by liquids, the local thermal efficiency at nominal conditions can be estimated as function of the nominal DNI and the local HTF temperature inside the troughs [34]:

$$\eta_{PTC,l}\,(\%) = -0.00013 \cdot \mathrm{T}^2\ (^\circ\mathrm{C}) + 0.0313 \cdot \mathrm{T}\ (^\circ\mathrm{C}) + 69.563 \tag{9}$$

The whole solar field comprises a set of parallel loops containing several ET-150 PTC in series with a nominal HTF mass flow rate of 7.725 kg/s. The number of parallel loops and collectors in series are selected to achieve the desired thermal power at the corresponding operating conditions.

These conditions are linked to the SSG design and operation. Particularly, SSG simulation is based on the heat balance. The pinch point is established in 10 K, which is reached at its cold-end. Thus, the minimum HTF temperature is determined by the saturation temperature of the high-pressure level and the pinch point, while the maximum HTF temperature is fixed at 390 °C.

To calculate the number of PTC in series within each loop, the following equations can be used:

$$\begin{cases} d\dot{Q} = \dot{m}_{HTF,loop,des} \cdot dh \\ d\dot{Q} = \eta_{PTC,l}\,(\mathrm{T}) \cdot (DNI \cdot IAM) \cdot dA_{col} = \eta_{PTC,l}\,(\mathrm{T}) \cdot (DNI \cdot IAM) \cdot W_{col} dL \end{cases} \tag{10}$$

The length required for the required HTF temperature variation is:

$$dL = \frac{\dot{m}_{HTF,loop,des}}{(DNI \cdot IAM) \cdot W_{col}} \cdot \frac{c_p \cdot dT}{\eta_{PTC,l}\,(\mathrm{T})} \Rightarrow L_{col} = \frac{\dot{m}_{HTF,l0op,des}}{(DNI \cdot IAM) \cdot W_{col}} \cdot \int_{T_i}^{T_o} \frac{c_p \cdot dT}{\eta_{PTC,l}\,(\mathrm{T})} \tag{11}$$

In this work, the HTF is Therminol VP1. Its properties are taken from Ref. [35].

As the unitary length of the ET-150 is known, the number of collectors should approximated to the upper integer number resulting from dividing the result of Equation (22) by the ET-150 length. Likewise, the number of loops should be the upper integer number resulting from dividing the desired thermal power by the thermal power of the unitary loop.

For the off-design operation, the thermal efficiency of the solar collector is calculated with the heat balances while the value of the DNI is corrected with the incidence angle modifier [33]. The oil outlet temperature of the solar field is maintained constant at all time. Thus, off-design operation conveys the HTF mass flow rate regulation. In order to ensure a correct cooling of the troughs, a minimum DNI of 300 W/m^2 is established for the solar field to operate.

Regarding the SSG, for the off-design operation, the heat balance and the thermal conductance are used, similarly to Equation (4) for recuperators. In this case, with fluids with a Pandtl from 5 to 7, the variation of U is governed by an exponent 0.8, so Equation (5) becomes:

$$U \Big/ U_{des} = \left(\dot{m}_{HTF} / \dot{m}_{HTF,des}\right)^{0.8} \tag{12}$$

The complete simulation code was developed in Ref. [36]. Details and validation can also be found in Refs. [37,38].

4.4. Site for the plant and yearly simulation

Annual yield and fuel consumption depend on the site where the plant is installed. In previous works [22,23,39], the yearly behaviour of several ISCCs has been studied in Almeria and in Las Vegas. Both sites are maintained in the present work to investigate for the first time the behaviour of the ISCC-PR configuration. Both sites have similar latitude, but climate in Las Vegas is more favourable for CSP and, conversely, in Almeria it is better for CCGT, owing to lower temperature variation ranges.

Simulations are carried out in hourly basis, taking into account the ambient conditions and the corrected solar irradiation (product *DNI·IAM*) during a typical meteorological year (TMY). The complete simulation conveys 8760 calculating points. In order to reduce this number, the methodology described and validated in Refs. [22] is used. Specifically, the methodology is based in a frequency matrix that contains the number of hours that each ambient condition is repeated along the TMY. This leads to 538 points in the case of Almeria and 909 in Las Vegas. Fig. 4 shows, as an example, the matrix for the case of Almeria.

4.5. Figures of merit

Annual yield can be calculated as the sum of the hours at each operating condition times the power at such condition. Thus, thermal efficiency, which is the ratio of total production to supplied energy (both fossil and solar), can be calculated as below:

$$\eta = \frac{\sum n \cdot t \cdot (P_{gt} + P_{st})}{\sum n \cdot t \cdot \left(\dot{m}_f \cdot H_c + \dot{Q}_{sol,\mathrm{gross}}\right)} \tag{13}$$

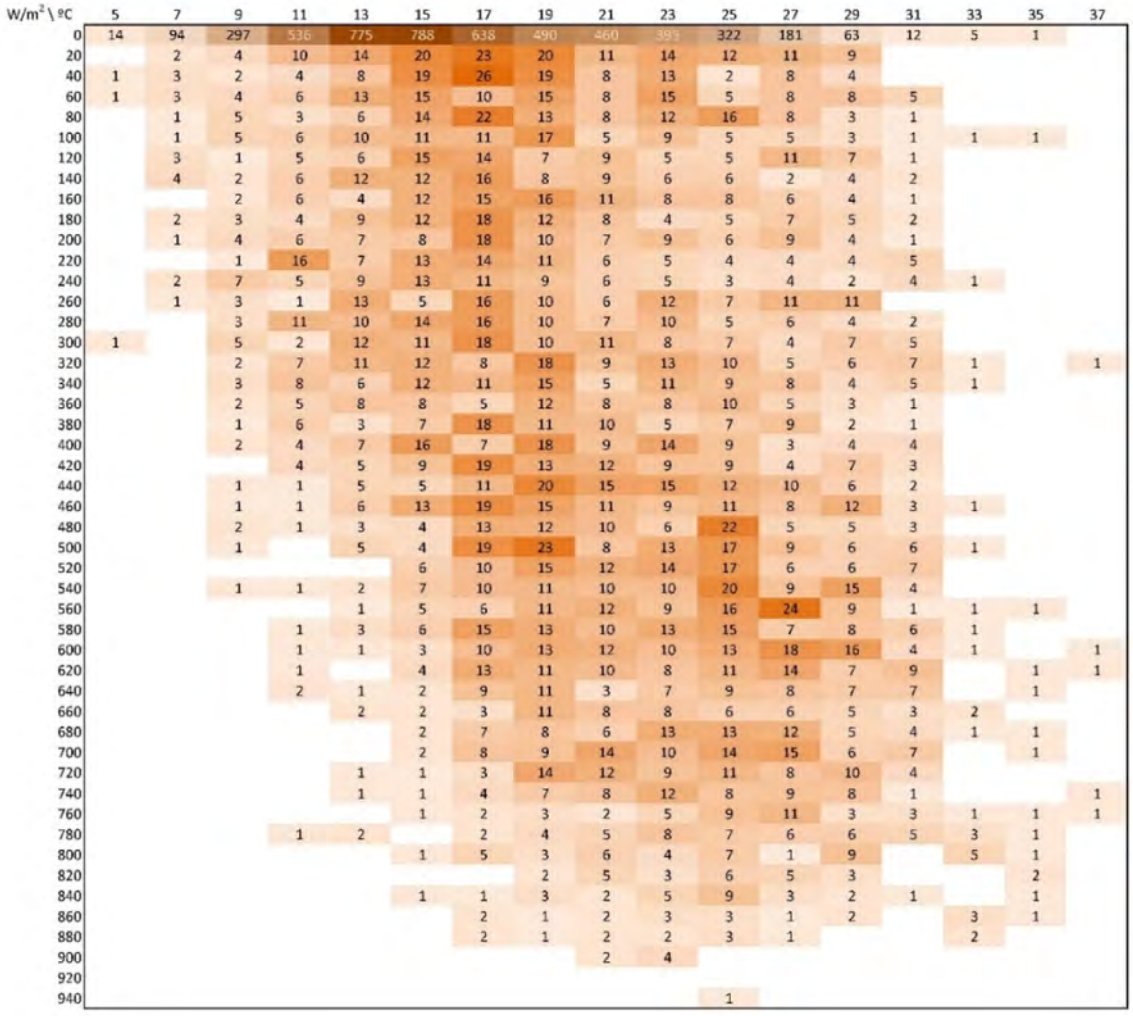

W/m² \ ºC	5	7	9	11	13	15	17	19	21	23	25	27	29	31	33	35	37
0	14	94	297	536	775	788	638	490	460	393	322	181	63	12	5	1	
20		2	4	10	14	20	23	20	11	14	12	11	9				
40	1	3	2	4	8	19	26	19	8	13	2	8	4				
60	1	3	4	6	13	15	10	15	8	15	5	8	8	5			
80		1	5	3	6	14	22	13	8	12	16	8	3	1			
100		1	5	6	10	11	11	17	5	9	5	5	3	1	1	1	
120		3	1	5	6	15	14	7	9	5	5	11	7	1			
140		4	2	6	12	12	16	8	9	6	6	2	4	2			
160			2	6	4	12	15	16	11	8	8	6	4	1			
180		2	3	4	9	12	18	12	8	4	5	7	5	2			
200		1	4	6	7	8	18	10	7	9	6	9	4	1			
220			1	16	7	13	14	11	6	5	4	4	4	5			
240		2	7	5	9	13	11	9	6	5	3	4	2	4	1		
260		1	3	1	13	5	16	10	6	12	7	11	11				
280			3	11	10	14	16	10	7	10	5	6	4	2			
300	1		5	2	12	11	18	10	11	8	7	4	7	5			
320			2	7	11	12	8	18	9	13	10	5	6	7	1		1
340			3	8	6	12	11	15	5	11	9	8	4	5	1		
360			2	5	8	8	5	12	8	8	10	5	3	1			
380			1	6	3	7	18	11	10	5	7	9	2	1			
400			2	4	7	16	7	18	9	14	9	3	4	4			
420				4	5	9	19	13	12	9	9	4	7	3			
440			1	1	5	5	11	20	15	15	12	10	6	2			
460			1	1	6	13	19	15	11	9	11	8	12	3	1		
480			2	1	3	4	13	12	10	6	22	5	5	3			
500			1		5	4	19	23	8	13	17	9	6	6	1		
520						6	10	15	12	14	17	6	6	7			
540			1	1	2	7	10	11	10	10	20	9	15	4			
560					1	5	6	11	12	9	16	24	9	1	1	1	
580				1	3	6	15	13	10	13	15	7	8	6	1		
600				1	1	3	10	13	12	10	13	18	16	4	1		1
620				1		4	13	11	10	8	11	14	7	9		1	1
640				2	1	2	9	11	3	7	9	8	7	7		1	
660					2	2	3	11	8	8	6	6	5	3	2		
680						2	7	8	6	13	13	12	5	4	1	1	
700						2	8	9	14	10	14	15	6	7		1	
720					1	1	3	14	12	9	11	8	10	4			
740					1	1	4	7	8	12	8	9	8	1			1
760						1	2	3	2	5	9	11	3	3	1	1	1
780				1	2		2	4	5	8	7	6	6	5	3	1	
800						1	5	3	6	4	7	1	9		5	1	
820								2	5	3	6	5	3			2	
840						1	1	3	2	5	9	3	2	1		1	
860							2	1	2	3	3	1	2		3	1	
880							2	1	2	2	3	1			2		
900									2	4							
920																	
940											1						

Fig. 4. Frequency matrix for Almeria TMY.

Although the worth of the thermal efficiency is clear in conventional and non-hybrid systems, it is not the best parameter in plants involving two energy sources. Particularly, in the case of ISCC the use of thermal efficiency has two drawbacks: it does not account for the contribution of each source; and it penalises the solar contribution (because it is introduced in the bottoming cycle, with lower efficiency), which is not congruent with the objective of plant.

An alternative to the thermal efficiency for this kind of systems is the heat rate (*HR*), which is the inverse of the efficiency, but only considering the fossil fuel consumption:

$$HR = \frac{\sum n \cdot t \cdot \dot{m}_f \cdot H_c}{\sum n \cdot t \cdot (P_{gt} + P_{st})} \tag{14}$$

Another choice is the use of the incremental solar-to-electricity efficiency [5], which is the ratio of the incremental production (due to the solar contribution) to the supplied solar energy. This efficiency is useful to compare ISCC to pure CSP:

$$\eta_{inc} = \frac{\sum n \cdot t \cdot \left((P_{gt} + P_{st})_{ISCC} - (P_{gt} + P_{st})_{CCGT} \right)}{\sum n \cdot t \cdot \dot{Q}_{sol,gross}} \tag{15}$$

However, the incremental efficiency has only sense in the cases of plants operating with boosting strategy, but not operating at fuel saving mode because, in such case, the numerator of Equation (15) becomes null. At this regard, different approaches have been proposed in order to modify the incremental efficiency. For example, Refs. [8,24] allocate the contribution of each source, leading to the expression below:

$$E_{sol-elec} = \sum n \cdot t \cdot \left(\Delta P - \eta_{CCGT} \cdot \Delta \dot{m}_f \cdot H_C \right) \tag{16}$$

where ΔP is the incremental power of the ISCC configuration over the CCGT one.

Therefore, the solar-to-electricity efficiency is:

$$\eta_{sol-elec} = \frac{\sum n \cdot t \cdot \left(\Delta P - \eta_{CCGT} \cdot \Delta \dot{m}_f \cdot H_C \right)}{\sum n \cdot t \cdot \dot{Q}_{sol,gross}} \tag{17}$$

This efficiency depends on a reference configuration without solar contribution, so the selection of a suitable reference is mandatory. This fact introduces some uncertainty because this reference is a choice of the analyst.

In order to define a figure of merit that does not depend on a reference but on its own layout, a new efficiency is proposed, which weights the energy contribution of each source considering their

exergy supply. Exergy supplied by the fossil resource to the cycle can be assessed with the following equation:

$$\dot{E}_{f\rightarrow cycle} = \dot{m}_g \cdot e_{g3} - \dot{m}_a \cdot e_{g2} \tag{18}$$

where g_2 should be replaced by g_{2R} in the ISCC-PR configuration.

Similarly, exergy transferred from the solar field to the cycle is:

$$\dot{E}_{PTC\rightarrow cycle} = \dot{m}_{SSG} \cdot (\Delta e_{HTF}) \tag{19}$$

Note that the above exergy fluxes correspond to the exergy transferred to the system, so they are not the exergy received from the source, i.e. the exergy losses in the combustion chamber and the solar field (the highest ones, and of different nature one to the other) are discounted.

The power fraction attributed to the solar contribution, namely the internal solar to electricity production (E_{ise}), is:

$$E_{ise} = \sum \left(\frac{n \cdot t \cdot (P_{gt} + P_{st}) \cdot \dot{E}_{PTC\rightarrow cycle}}{\dot{E}_{f\rightarrow cycle} + \dot{E}_{PTC\rightarrow cycle}} \right) \tag{20}$$

Finally, the internal solar-to-electricity efficiency is defined as the ratio of internal solar to electricity production to the total energy supply:

$$\eta_{ise} = \frac{\sum \left(\frac{n \cdot t \cdot (P_{gt} + P_{st}) \cdot \dot{E}_{PTC\rightarrow cycle}}{\dot{E}_{f\rightarrow cycle} + \dot{E}_{PTC\rightarrow cycle}} \right)}{\sum n \cdot t \cdot \dot{Q}_{sol,gross}} \tag{21}$$

This figure of merit is similar to that proposed in Ref. [40], where authors present a methodology to allocate the power associated to different resources in hybrid plants. Specifically, the methodology consists on the identification of the irreversibility that affects to each resource, which is removed from the gross exergy coming from the corresponding heat source. Irreversibility of equipment not clearly devoted a specific source are weighted. Thus, the proposed figure of merit can be considered as a simplification of the methodology developed in Ref. [40].

All the above efficiencies can be calculated using either the gross solar thermal power (radiation collected by the mirrors) or net solar thermal power (energy transferred to the HTF). The ratio of net to gross solar thermal energy is the efficiency of the PTC:

$$\eta_{PTC} = \frac{\sum n \cdot t \cdot \dot{Q}_{sol,net}}{\sum n \cdot t \cdot \dot{Q}_{sol,gross}} \tag{22}$$

Regarding the economic assessment, the levelized cost of electricity (LCOE) is used:

$$LCOE = \frac{LC_{Inv} + LC_{O\&M} + LC_f}{E_{yearly}} \tag{23}$$

Table 3 shows the economical parameters used in the work.

In addition to the LCOE, the incremental solar cost can be also used, which is defined as below:

$$C_{inc-sol} = \frac{(LC_{Inv} + LC_{O\&M})_{ISCC} - (LC_{Inv} + LC_{O\&M})_{CCGT}}{E_{sol-elec}} \tag{24}$$

The denominator of Equation (24) can be replaced by the internal solar-to-electricity production, leading to the definition of the internal solar-to-electricity cost:

$$C_{ise} = \frac{(LC_{Inv} + LC_{O\&M})_{ISCC} - (LC_{Inv} + LC_{O\&M})_{CCGT}}{E_{ise}} \tag{25}$$

5. Results

5.1. Performance of the reference and proposed configurations at nominal operation

Table 4 shows the performance of the different configurations at nominal conditions: the capacity of the steam turbines, the thermal conductance of the heat exchangers and the size and efficiency of the solar field.

As it is observed, solar integration in the reference ISCC, that is fixed at 16 MWth, allows an increase of the nominal power over the reference CCGT that results in 130 MWe instead of 125 MWe, due to a higher power rate of the steam cycle. For that reason, the capacity of the steam turbine should be increased. Also, the heat exchangers of the high-pressure level of the HRSG should be larger than in the reference CCGT configuration, as they work with higher steam mass flow rates.

Solar thermal input in ISCC-PR configuration at nominal conditions is the same as in the reference ISCC (i.e. 16 MWth). However, as the steam production does not vary significantly, the nominal power rate of the plant is lower than in the reference ISCC and roughly the same as in the reference CCGT (slightly lower due to the additional pressure drop in the recuperator). Thus, in this case, the capacity of the steam turbine is the same than in the reference CCGT configuration. Likewise, the size of the heat exchangers corresponding to the HRSG high-pressure level is similar to that of the CCGT except for the high-pressure superheater, which requires a higher thermal conductance because the gas-to-steam temperature difference is kept constant along the heat exchanger. In fact, the superheater requires lower mean temperature difference to achieve the same heat transfer because part of the gas mass flow rate is directed to the recuperator.

5.2. Performance of the reference and proposed configurations at off-design operation

Table 5 shows the performance results obtained for the reference CCGT, reference ISCC and ISCC-PR at different operating conditions.

As previously commented, ambient temperature significantly affects the CCGT performance. At high temperatures, air density is low, and the power rate decreases. Reference ISCC configuration has a steam turbine with larger capacity, since at nominal conditions the SSG increases the steam mass flow rate. Likewise, the high-pressure level superheater and economisers are larger than in the reference CCGT configuration (Table 4). This fact mitigates the previous one since higher heat exchange areas convey higher steam production. As a result, the performance of the reference ISCC at conditions with null or low solar irradiation is slightly poorer than the reference CCGT's owing to two reasons: the isentropic efficiency of the steam turbine is penalised due to the part load operation and the working pressure is lower.

When solar irradiation is high, the power rate of the ISCC is higher and, consequently, the *HR* improves. Besides, the steam turbine is closer to its nominal working condition. Regarding the solar efficiencies, the solar-to-electricity efficiency reaches values from 36% to 40% in net term or 23%–26% in gross term. The internal solar-to-electricity efficiency reaches very similar values. Thus, this figure of merit, which does not depend on any reference

Table 3
Economic data [22].

Land cost	2 €/m^2
Solar field cost	200 €/m^2
Surcharge for construction, engineering and contingencies	10%
Specific cost for the power block [41,42]	(466,1 + 113900/P [MW]) €/kW
Steam turbine cost variation (based on [25])	(0,207·ΔP [MW]) M€
SSG cost [13] [a]	(−0,0007·A^2 [m^2]+126,9 A [m^2]+7770,4) €
Gas turbine's recuperator cost [43] [a]	(2861·$A^{0.59}$ [m^2]) $
Solar field O&M cost	9 €/(year·m^2)
Combined cycle O&M cost	17,9 €/(year·kW)
Yearly O&M equipment cost percentage of Inv.	1% · Inv
Interest rate	4%
Life	25 years
O&M Escalation rate	1%
Fuel escalation rate	2.5%
Price of natural gas	2.32 c€/kWh

[a] The considered convective heat transfer coefficients for the SSG and recuperator are 1500 W/(m^{2}K) and 700 W/(m^{2}K), respectively [43,44].

Table 4
Performance of the configurations at nominal operation.

	Reference CCGT	Reference ISCC	ISCC-PR
P	124.8 MW	130.1 MW	123.0 MW
η	53.2%	52.0%	53.2%
P_{gt}	87.7 MW	87.7 MW	86.0 MW
P_{st}	37.1 MW	42.4 MW	37.0 MW
$\dot{m}_f H_c$	234.4 MW	234.4 MW	214.9 MW
HP turbine capacity	$9.0\cdot10^{-5}$ m K$^{0.5}$ s	$11.3\cdot10^{-5}$ m K$^{0.5}$ s	$9.1\cdot10^{-5}$ m K$^{0.5}$ s
LP turbine capacity	$1.531\cdot10^{-3}$ m K$^{0.5}$ s	$1.534\cdot10^{-3}$ m K$^{0.5}$ s	$1.538\cdot10^{-3}$ m K$^{0.5}$ s
$UA_{sh,HP}$	218.3 kW/K	272.9 kW/K	528.8 kW/K
$UA_{ev,HP}$	713.4 kW/K	713.4 kW/K	714.8 kW/K
$UA_{sh,LP}$	38.5 kW/K	38.5 kW/K	38.2 kW/K
$UA_{ec,HP}$	367.2 kW/K	459.0 kW/K	370.0 kW/K
$UA_{ev,LP}$	448.9 kW/K	448.9 kW/K	447.5 kW/K
$UA_{ec,HP\text{-}LP}$	209.2 kW/K	261.5 kW/K	210.2 kW/K
UA_{SSG}	–	454.0 kW/K	454.0 kW/K
UA_R	–	–	480.3 kW/K
Mirrors area	–	29,456 m^2	29,456 m^2
Land requirement	–	83,798 m^2	83,798 m^2
Solar efficiency	–	64.4%	64.4%

Table 5
Performance of the configurations at off-design operation.

		P (MW)	P_{GT} (MW)	P_{ST} (MW)	$\dot{m}_f H_c$ (MW)	$Q_{sol,net}$ (MW)	HR	η	$\eta_{sol\text{-}elec}$	η_{ise}	p_{max} (bar)
0 °C	CCGT	137.7	99.0	38.7	255	–	1.85	54.1%	–	–	91
0 W/m^2	ISCC	136.7	99.0	37.7	255	0	1.86	53.7%	–	–	75
	ISCC-PR	136.8	97.9	38.9	255	0	1.86	53.9%	–	–	91
15 °C	CCGT	124.8	87.7	37.1	234	–	1.88	53.2%	–	–	90
0 W/m^2	ISCC	123.9	87.7	36.2	234	0	1.89	52.9%	–	–	75
	ISCC-PR	124.1	86.8	37.3	234	0	1.88	53.1%	–	–	90
30 °C	CCGT	109.0	73.8	35.2	210	–	1.93	51.9%	–	–	89
0 W/m^2	ISCC	108.2	73.8	34.4	210	0	1.94	51.5%	–	–	73
	ISCC-PR	108.6	73.2	35.4	210	0	1.93	51.8%	–	–	89
0 °C	ISCC	142.2	99.0	43.2	255	13.8	1.79	53.0%	39.6%	40.5%	89
725 W/m^2	ISCC-PR	136.9	98.3	38.7	239	13.8	1.75	54.2%	59.3%	41.2%	90
15 °C	ISCC	130.1	87.7	42.4	234	16.1	1.80	52.0%	38.7%	38.8%	90
850 W/m^2	ISCC-PR	123.0	86.0	37.0	215	16.1	1.75	53.2%	55.3%	39.3%	89
30 °C	ISCC	114.4	73.8	40.5	210	16.1	1.84	50.6%	38.2%	36.6%	89
850 W/m^2	ISCC-PR	107.9	72.8	35.1	191	16.1	1.77	52.0%	55.1%	37.1%	88

configuration, can be considered as suitable.

Finally, ISCC-PR configuration does not require a larger steam turbine or economisers (see Table 4), because the additional thermal power supplied by the SSG is mitigated by lower thermal energy coming from the exhaust gas of the gas turbine, which has exchanged some energy in the recuperator. However, the high-pressure superheater is larger in order to achieve the required thermal exchange with lower gas mass flow rate and lower mean temperature difference.

Comparing the performance of ISCC-PR to that of CCGT when there is not solar irradiation, one may observe that both power rate and *HR* are very similar. CCGT results are slightly better than ISCC-PR ones due to the additional pressure drop in the recuperator. Comparing ISCC-PR to the reference ISCC at null solar irradiation, one may observe that both power rate and *HR* are also very similar but, in this case ISCC-PR performance is better, since it works closer

to its nominal conditions (steam turbine is not over-sized).

With high solar irradiation, the ISCC-PR reaches roughly the same power as the reference CCGT and lower than reference ISCC. However, *HR* improves due to the lower fuel consumption without any incidence in the gas turbine power. Regarding the solar efficiencies, it is observed that the solar-to-electricity efficiency reaches values above 55% (in net term), because each unit of net solar energy contribution equals a unit of net fuel energy contribution. Thus, the configuration behaves like if the solar heat is introduced in the gas turbine instead of in the steam cycle.

On the other hand, the internal solar-to-electricity efficiency of ISCC-PR is also higher than that obtained with the reference ISCC, reaching 40% (net term), but the improvement is less sound in this case. This is due to a fair assessment of the efficiency taking into account the quality of the solar heat supplied by means of an exergy weighting. In fact, the energy saved from the fossil contribution is equal to the solar energy supplied, but it is transferred to the air before the combustion, while the fuel contribution is still responsible for the high temperatures reached in the gas turbine. For that reason, to the authors' opinion, the internal solar-to-electricity efficiency can measure more fairly the performance than the conventional solar-to-electricity efficiency.

5.3. Daily and yearly operation

As an example, Fig. 5 depicts the results obtained by the models during a summer day (June 27th) in Las Vegas, when the maximum DNI is approximately 900 W/m^2. One may observe that, in a sunny day, the daily maximum power output is obtained around 5 a.m., when the ambient temperature is minimum, which maximizes the air flow at the gas turbine and minimizes the condenser pressure. Power output is the same for CCGT and ISCC-PR configurations, whereas it is higher for reference ISCC during high irradiation periods.

Regarding the fuel consumption and *HR*, while for CCGT low ambient temperatures lead to a better performance, in the case of ISCCs high irradiation allows lower *HR*, compensating the adverse effect of the high ambient temperature. It is interesting to observe that the ISCC-PR is able to minimize fuel consumption during these hours and becomes the best configuration in terms of *HR* performance.

Finally, Fig. 6 shows the detail of the air and gas mass flow rate that is directed to the recuperator, the bypasses and the high pressure superheaters.

Regarding the yearly behaviour, Fig. 7 shows the energy production, the consumption and the heat rate of the different configurations for the sites of Almeria and Las Vegas. The reference CCGT has a better performance in Almeria than in Las Vegas due to lower temperatures. On the other hand, reference ISCC and ISCC-PR configurations behave better in Las Vegas, due to a higher solar contribution. Particularly, the heat rate reached by the ISCC-PR configuration is the best in both sites.

Fig. 8 shows the solar energy received and collected (considering only the periods with DNI higher than 300 W/m^2), the solar-to-electricity energy conversion, the internal solar-to-electricity conversion and the corresponding efficiencies. It is interesting to note that the solar resource is much more favourable in Las Vegas, which supports the better performance of the reference ISCC and ISCC-PR configurations in this site. Besides, the values of the internal solar-to-electricity production and efficiency are more constant than the conventional solar-to-electricity ones, which depends on the reference configuration. Once again, the internal figures of merit seem more reliable and fairer since they provide similar values to technologies that provide the thermal energy at the same level of temperature. Finally, it is observed that the highest values of solar-to-energy conversion and efficiencies are achieved by the proposed ISCC-PR configuration.

Finally, Fig. 9 shows the LCOE, the solar incremental cost and the internal solar-to-electricity cost. In the proposed scenario, solar integration with the conventional technology, i.e. reference ISCC configuration, does not introduce advantages and the increase of production does not compensate the increase in capital expenditure. However, the ISCC-PR configuration is feasible if it is compared to the reference ISCC and it even reduces the LCOE in sites with favourable climate like Las Vegas. In this site, the ISCC-PR configuration reaches the lowest LCOE.

To complete the information, Table 6 shows the most important data for the economic analysis.

It is important to highlight that the good economic results of ISCC-PR are supported by the fact that this configuration works close to its nominal condition at all time, because neither the gas turbine nor the steam turbine load vary to a large extent. On the contrary, the reference ISCC suffers from steam turbine load variation along with the solar irradiation variation, which has some incidence on the performance.

Regarding the incremental costs, the lowest values are obtained for the ISCC-PR configuration. Besides, the internal solar-to-electricity cost defined in this work is more constant than the conventional incremental solar cost, which varies significantly from one technology to another. Thus, it can be concluded that the figures of merit defined in the work provide fair and reliable results for solar hybrid systems like ISCCs.

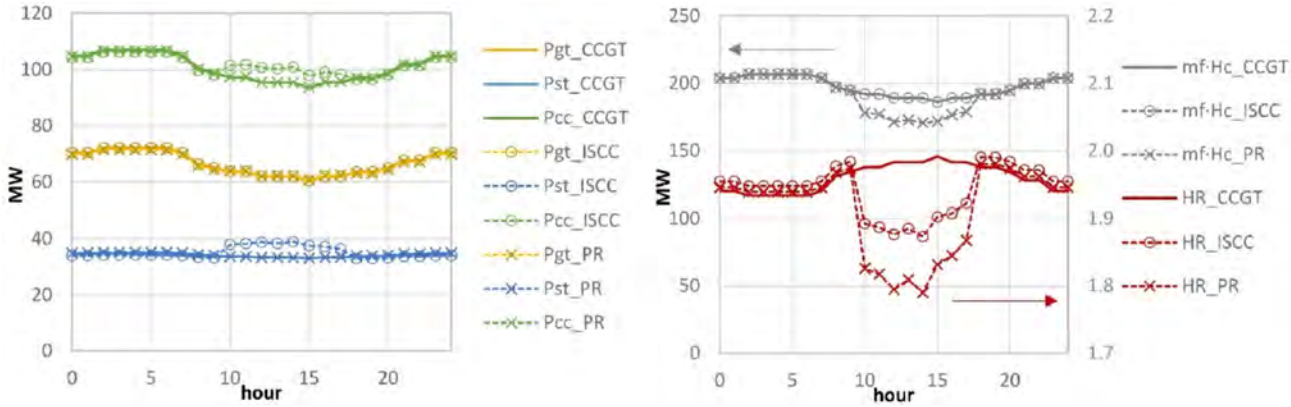

Fig. 5. Power output of plant components (left) and fuel thermal power input and heat rate (right) for the three configurations.

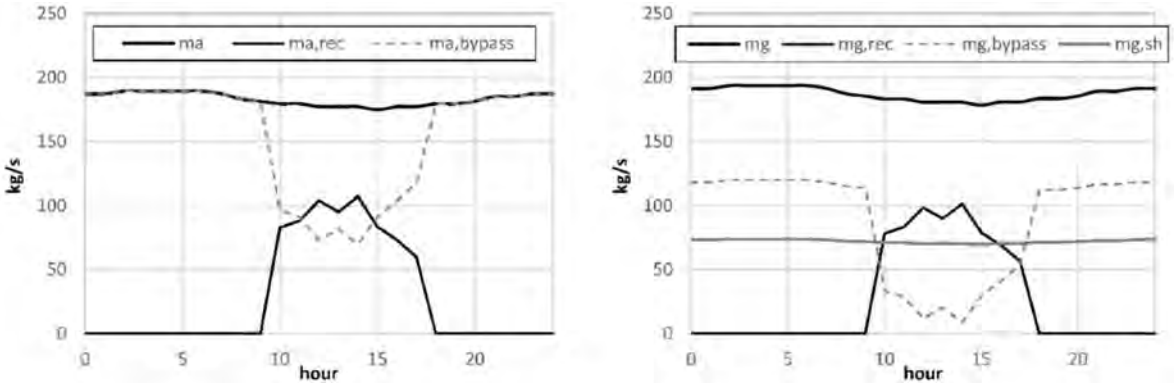

Fig. 6. Air mass flow directed to the recuperator and bypass (left) and gas mass flow directed to the recuperator, bypass and HP superheater (right).

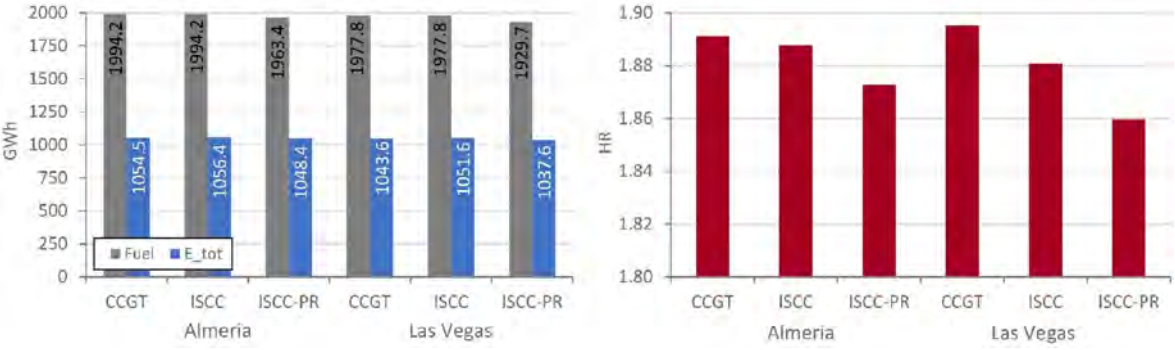

Fig. 7. Yearly energy production and consumption (left) and heat rate (right) for the three configurations in Almeria and Las Vegas.

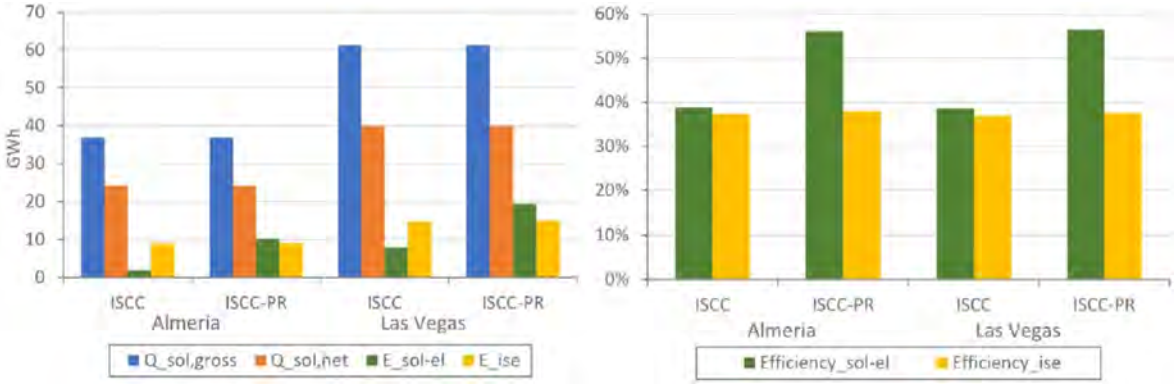

Fig. 8. Solar-to-energy energy conversion (left) and efficiencies (right) for the three configurations in Almeria and Las Vegas.

6. Conclusions

In this paper, a new configuration for integrated solar combined cycle plants with partial recuperation has been proposed. This configuration seeks an improved use of the solar source when it is available and low inefficiencies when it is unavailable.

At high irradiation conditions, the proposed ISCC-PR configuration achieves a better performance than conventional ISCC. The improvement is given by a better use of the solar heat input, which allows a fuel saving proportionally to this solar input. Specifically, the heat rate is reduced roughly a 2.5%, which conveys a thermal efficiency increase of 1.2% point. At conditions without solar irradiation, ISCC-PR also achieves better performance since the steam cycle nominal power is the same as in the reference CCGT and, thus, it is not working at part load when the solar source is not available. In this case, the incremental percentage points in thermal efficiency is about 0.2 points.

Two case studies have been compared: Las Vegas and Almeria. The minimum yearly heat rate has been achieved by the proposed ISCC-PR configuration compared to the state-of-the-art CCGT (improvement of 1.0% and 1.8% in Almeria and Las Vegas, respectively) and ISCC configurations (0.8% and 1.1%, respectively).

Regarding the cost analysis, ISCC-PR configuration achieves a lower LCOE than the ISCC case both in Almeria and Las Vegas (0.9% and 1.1%, respectively) and a lower solar-to-electricity cost (about 35% in both cases). Furthermore, whereas ISCC is never able to reduce the LCOE compared to a CCGT (it increases a 1.0% in Almeria and 0.4% in Las Vegas), ISCC-PR minimizes the increase in Almeria

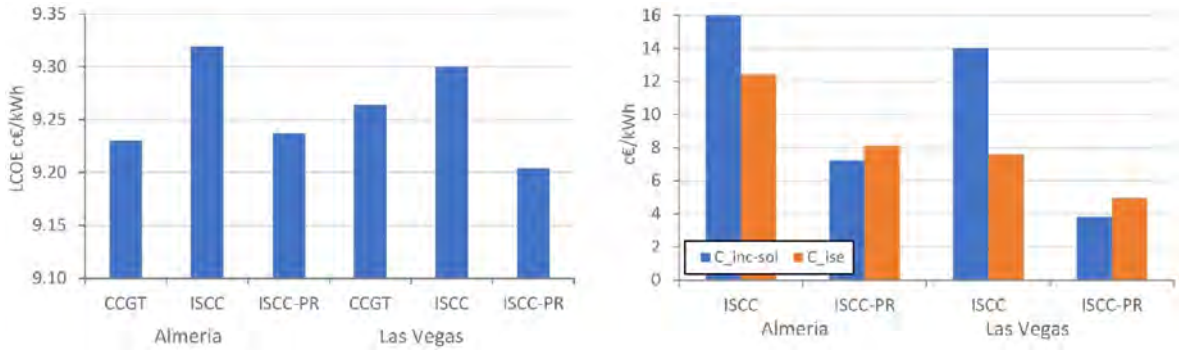

Fig. 9. LCOE (left), incremental solar cost and internal solar-to-electricity costs (right) for the three configurations in Almeria and Las Vegas.

Table 6
Economic results and data.

	Almeria							
	P (MW)	Inv (M€)	LC_{Inv} (M€)	$LC_{o\&m}$ (M€)	LC_f (M€)	LCOE (c€/kWh)	$C_{inc\text{-}sol}$ (c€/kWh)	C_{ise} (c€/kWh)
CCGT	125	189.4	12.1	5.9	79.4	9.23	–	–
ISCC	132	197.1	12.6	6.5	79.4	9.32	57.70	12.44
ISCC-PR	123	195.2	12.5	6.2	78.1	9.24	7.24	8.12
Las Vegas								
CCGT	125	189.4	12.1	5.9	78.7	9.26	–	–
ISCC	132	197.1	12.6	6.5	78.7	9.30	14.03	7.59
ISCC-PR	123	195.2	12.5	6.2	76.8	9.20	3.81	4.94

(0.1% higher than CCGT) and reduces it in Las Vegas (0.6% lower than CCGT).

Finally, the authors outline the advantages of the internal solar-to-electricity efficiency, developed in this paper, compared to the solar-to-electricity efficiency. Indeed, the new concept is less variable for different configurations and does not depend on the reference configuration used.

Declaration of competing interests

The authors declare that they have no known competing financial interests or personal relationships that could have appeared to influence the work reported in this paper.

Acknowledgments

This work has been supported by the Spanish Ministry of Economy and Competitiveness through the ENE2015-70515-C2-1-R and ENE2015-70515-C2-2-R projects.

References

[1] Allani Y, Favrat D, von Spakovsky MR. CO_2 mitigation through the use of hybrid solar-combined cycles. Energy Convers Manag 1997;38:s661–7. org/10.1016/S0196-8904(97)00012-5.
[2] Baghernejad A, Yaghoubi M. Exergy analysis of an integrated solar combined cycle system. Renew Energy 2010;35:2157–64. org/10.1016/j.renene.2010.02.021.
[3] Behar O, Khellaf A, Mohammedi K, Ait-Kaci S. A review of integrated solar combined cycle system (ISCCS) with a parabolic trough technology. Renew Sustain Energy Rev 2014;39:223–50. org/10.1016/j.rser.2014.07.066.
[4] Alqahtani BJ, Patiño-Echeverri D. Integrated solar combined cycle power plants: paving the way for thermal solar. Appl Energy 2016;169:927–36. org/10.1016/j.apenergy.2016.02.083.
[5] Dersch J, Geyer M, Herrmann U, Jones SA, Kelly B, Kistner R, Ortmanns W, Pitz-Paal R, Price H. Trough integration into power plants—a study on the performance and economy of integrated solar combined cycle systems. Energy 2004;29:947–59. org/10.1016/S0360-5442(03)00199-3.
[6] Falchetta M, Mazzei D, Crescenzi T, Merlo L. Design of the Archimede 5MW molten salt parabolic trough solar plant. In: Proceedings of the SolarPACES; 2009. Berlin, Germany, 15–18 September 2009.
[7] Nezammahalleh H, Farhadi F, Tanhaemami M. Conceptual design and techno-economic assessment of integrated solar combined cycle system with DSG technology. Sol Energy 2010;84:1696–705. org/10.1016/j.solener.2010.05.007.
[8] Li Y, Yang Y. Thermodynamic analysis of a novel integrated solar combined cycle. Appl Energy 2014;122:133–42. org/10.1016/j.apenergy.2014.02.017.
[9] Cau G, Cocco D, Tola V. Performance and cost assessment of Integrated Solar Combined Cycle Systems (ISCCSs) using CO2 as heat transfer fluid. Sol Energy 2012;86:2975–85. org/10.1016/j.solener.2012.07.004.
[10] Baghernejad A, Yaghoubi M. Multi-objective exergoeconomic optimization of an integrated solar combined cycle system using evolutionary algorithms. Int J Energy Res 2011;35:601–15. org/10.1002/er.1715.
[11] El Jai MC, Chalqui FZ. A modified model for parabolic trough solar receiver. Am. J. Eng. Res. 2013;2:200–11.
[12] Abdel Dayem AM, Nabil Metwally M, Alghamdi AS, Marzouk EM. Numerical simulation and experimental validation of integrated solar combined power plant. Energy Procedia 2014;50:290–305. org/10.1016/j.egypro.2014.06.036.
[13] Griffin P, Huschka K, Morin G. Software for design, simulation, and cost estimation of solar thermal power and heat cycles. In: proceedings of the SolarPACES; 2009. Berlin, Germany, 15–18 September 2009.
[14] Calise F, d'Accadia MD, Libertini L, Vicidomini M. Thermoeconomic analysis of an integrated solar combined cycle power plant. Energy Convers Manag 2018;171:1038–51. org/10.1016/j.enconman.2018.06.005.
[15] Brodrick PG, Brandt AR, Durlofsky LJ. Operational optimization of an integrated solar combined cycle under practical time-dependent constraints. Energy 2017;141:1569–84. org/10.1016/j.energy.2017.11.059.
[16] Li Y, Xiong Y. Thermo-economic analysis of a novel cascade integrated solar combined cycle system. Energy 2018;145:116–27. org/10.1016/j.energy.2017.12.128.
[17] Bonforte G, Buchgeister J, Manfrida G, Petela K. Exergoeconomic and exergoenvironmental analysis of an integrated solar gas turbine/combined cycle power plant. Energy 2018;156:352–9. org/10.1016/j.energy.2018.05.080.
[18] Amelio M, Ferraro V, Marinelli V, Summaria A. An evaluation of the performance of an integrated solar combined cycle plant provided with air-linear parabolic collectors. Energy 2014;69:742–8. org/10.1016/j.energy.2014.03.068.
[19] Okoroigwe E, Madhlopa A. An integrated combined cycle system driven by a solar tower: a review. Renew Sustain Energy Rev 2016;57:337–50. doi.org/10.1016/j.rser.2015.12.092.
[20] Horn M, Führing H, Rheinländer J. Economic analysis of integrated solar combined cycle power plants: a sample case: the economic feasibility of an ISCCS power plant in Egypt. Energy 2004;29:935–45. org/10.1016/S0360-5442(03)00198-1.
[21] Duan L, Qu W, Jia S, Feng T. Study on the integration characteristics of a novel integrated solar combined cycle system. Energy 2017;130:351–64. org/10.1016/j.energy.2017.04.118.

[22] Rovira A, Barbero R, Montes MJ, Abbas R, Varela F. Analysis and comparison of Integrated Solar Combined Cycles using parabolic troughs and linear Fresnel reflectors as concentrating systems. Appl Energy 2016;162:990–1000. org/10.1016/j.apenergy.2015.11.001.
[23] Rovira A, et al. Comparison of different technologies for integrated solar combined cycles: analysis of concentrating technology and solar integration. Energies 2018;11:1064. org/10.3390/en11051064.
[24] Rovira A, Sánchez C, Fernández S, Muñoz M, Barbero R. Integrated solar combined cycles using gas turbines with partial recuperation and solar integration at different pressure levels. AIP Conference Proceedings 2017;1850:060004. org/10.1063/1.4984412.
[25] Rovira A, Sánchez C, Muñoz M. Analysis and optimisation of combined cycles gas turbines working with partial recuperation. Energy Convers Manag 2015;106:1097–108. org/10.1016/j.enconman.2015.10.046.
[26] Rovira A, Abbas R, Sánchez C, Muñoz M. Data for: Proposal and analysis of an integrated solar combined cycle with partial recuperation. Mendeley Data; 2019 [dataset].
[27] Walsh PP, Fletcher P. Gas turbine performance. 2[a] ed. Oxford: BlackWell Science; 2004.
[28] Stull DR, Prophet H. JANAF thermodynamic tables. NSRDS-NBS37; 1971.
[29] El-Gammal AM. An algorithm and criteria for compressor characteristics real time modeling and approximation. Trans. ASME, J. of Eng. for GT. and P. 1991;113:112–8. doi.org/10.1115/1.2906517.
[30] Stamatis A, Mathioudakis K, Papailiou KD. Adaptative simulation of gas turbine performance. Trans. ASME, J. of Eng. For GT. And P. 1990;112:168–75. doi.org/10.1115/1.2906157.
[31] El-Sayed YM. Revealing the cost-efficiency trends of the design concepts of Energy-Intensive Systems. Energy Convers Manag 1999;40:1599–615. org/10.1016/S0196-8904(99)00055-2.
[32] Manente G. High performance integrated solar combined cycles with minimum modifications to the combined cycle power plant design. Energy Convers Manag 2016;111:186–97. org/10.1016/j.enconman.2015.12.079.
[33] Montes MJ, Abánades A, Martínez-Val JM. Thermofluidynamic model and comparative analysis of parabolic trough collectors using oil, water/steam, or molten salt as heat transfer fluids. J Sol Energy Eng 2010;132(2):021001. org/10.1115/1.4001399.
[34] Rovira A, Montes MJ, Varela F, Gil M. Comparison of heat transfer fluid and direct steam generation technologies for integrated solar combined cycles. Appl Therm Eng 2013;52:264–74. doi.org/10.1016/j.applthermaleng.2012.12.008.
[35] Staff report. Technical bulletin 7239115C. Solutia. Available from: http://www.therminol.com/pages/products/vp-1.asp; 2008.
[36] Montes MJ, Rovira A, Muñoz M, Martínez-Val JM. Performance analysis of an integrated solar combined cycle using direct steam generation in parabolic trough collectors. Appl Energy 2011;88:3228–38. org/10.1016/j.apenergy.2011.03.038.
[37] Montes MJ. Análisis y propuestas de sistemas solares de alta exergía que emplean agua como fluido calorífero. PhD thesis. Madrid: Univ. Politécnica de Madrid; 2008 [in Spanish)].
[38] Rovira A, Montes MJ, Valdes M, Martínez-Val JM. Energy management in solar thermal power plants with double thermal storage system and subdivided solar field. Appl Energy 2011;88. https://doi.org/10.1016/j.apenergy.2011.04.036. 4055–12.
[39] Rovira A, Montes MJ, Valdes M, Martínez-Val JM, Varela F. On the improvement of annual performance of solar thermal power plants through exergy management. Int J Energy Res 2013. https://doi.org/10.1002/er.3075.
[40] Iora P, Beretta JP, Ghoniem AF. Exergy loss based allocation method for hybrid renewable-fossil power plants applied to an integrated solar combined cycle. Energy 2019;173:893–901. org/10.1016/j.energy.2019.02.095.
[41] Li Y, Yang Y. Impacts of solar multiples on the performance of integrated solar combined cycle systems with two direct steam generation fields. Appl Energy 2015;160:673–80. org/10.1016/j.apenergy.2015.08.094.
[42] Manente G, Rech S, Lazzaretto A. Optimum choice and placement of concentrating solar power technologies in integrated solar combined cycle systems. Renew Energy 2016;96:172–89. org/10.1016/j.renene.2016.04.066.
[43] Zare V, Mahmoudi SMS, Yari M. An exergoeconomic investigation of waste heat recovery from the Gas Turbine-Modular Helium Reactor (GT-MHR) employing an ammonia-water power/cooling cycle. Energy 2013;61:397–409. doi.org/10.1016/j.energy.2013.09.038.
[44] González-Gómez PA, Gómez-Hernández J, Briongos JV, Santana D. Fatigue analysis of the steam generator of a parabolic trough solar power plant. Energy 2018;155:565–77. doi.org/10.1016/j.energy.2018.04.193.